arXiv:2603.07113v1 [cs.CV] 7 Mar 2026

EFFICIENT CHEST X-RAY REPRESENTATION LEARNING VIA SEMANTIC-PARTITIONED CONTRASTIVE LEARNING

Wangyu Feng*
[1]Shenzhen University of Advanced Technology
Shenzhen, China

Shawn Young*
[1]Shenzhen University of Advanced Technology
Shenzhen, China

Lijian Xu†
Shenzhen University of Advanced Technology
Shenzhen, China
xulijian@suat-sz.edu.cn

March 10, 2026

ABSTRACT

Self-supervised learning (SSL) has emerged as a powerful paradigm for Chest X-ray (CXR) analysis under limited annotations. Yet, existing SSL strategies remain suboptimal for medical imaging. Masked image modeling allocates substantial computation to reconstructing high-frequency background details with limited diagnostic value. Contrastive learning, on the other hand, often depends on aggressive augmentations that risk altering clinically meaningful structures. We introduce **Semantic-Partitioned Contrastive Learning (S-PCL)**, an efficient pre-training framework tailored for CXR representation learning. Instead of reconstructing pixels or relying on heavy augmentations, S-PCL randomly partitions patch tokens from a single CXR into two non-overlapping semantic subsets. Each subset provides a complementary but incomplete view. The encoder must maximize agreement between these partitions, implicitly inferring global anatomical layout and local pathological cues from partial evidence. This semantic partitioning forms an internal bottleneck that enforces long-range dependency modeling and structural coherence. S-PCL eliminates the need for hand-crafted augmentations, auxiliary decoders, and momentum encoders. The resulting architecture is streamlined, computationally efficient, and easy to scale. Extensive experiments on large-scale CXR benchmarks, including ChestX-ray14, CheXpert, RSNA Pneumonia and SIIM-ACR Pneumothorax, show that S-PCL achieves competitive performance while attaining the lowest GFLOPs and superior accuracy among existing SSL approaches. The code is available at https://anonymous.4open.science/r/SPCL-C621.

Keywords Self-supervised Learning · Chest X-rays · Masked Image Modeling · Contrastive Learning · Efficient Pre-training.

1 Introduction

Self-supervised learning has become a central paradigm in medical image analysis by enabling representation learning from large-scale unlabeled data [1, 2]. Its effectiveness has been validated across classification, segmentation, and cross-domain transfer scenarios [3, 4], with subsequent studies demonstrating robustness and scalability in large medical corpora [5].

*Wangyu Feng and Shawn Young contributed equally to this work and conducted it during an internship at Shenzhen University of Advanced Technology.

†Corresponding author.

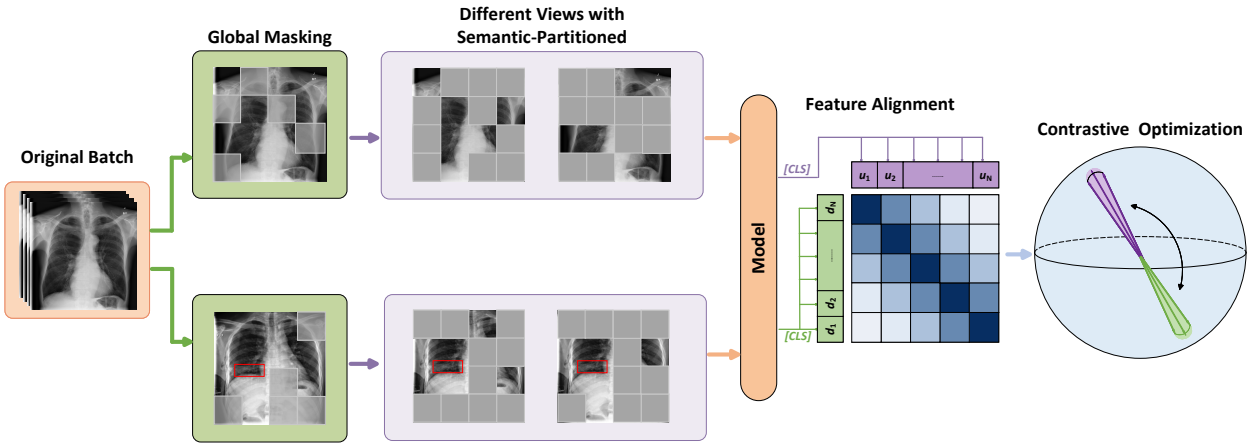

Figure 1: Our occluded image contrastive learning: Through non-overlapping occluding, distinct tokens within an image are categorized as intraclass, while across-image tokens within a batch are viewed as interclass.

Existing approaches largely fall into two categories: purely visual pretraining and vision language alignment. Within visual pretraining, image-level contrastive learning promotes instance discrimination and shows strong transferability [6, 7]. Masked image modeling instead learns contextual dependencies through reconstruction objectives [8], and has been extended to multi-scale and volumetric medical data [9, 10, 11]. Large-scale pretraining further improves performance across clinical benchmarks [12, 13]. Multimodal learning incorporates radiology reports to enhance semantic alignment [14, 15, 16]. Contrastive cross-modal strategies strengthen image–text correspondence [17, 18], while structured knowledge integration further refines chest X-ray representation [19, 20, 21]. Recently, efficient token compression has been widely studied to reduce computational overhead while preserving semantic content [22, 23, 24, 25, 26].

Despite these advances, current paradigms remain suboptimal for chest X-rays. Reconstruction-based objectives emphasize pixel fidelity [8, 27], often biasing models toward high-frequency textures. Contrastive frameworks rely on strong augmentations [6], which may distort subtle anatomical cues. Vision language approaches partially alleviate semantic ambiguity [14, 20], yet still depend on the stability of the underlying visual encoder. Taken together, existing strategies either optimize low-level reconstruction, enforce potentially unsafe invariances, or depend on auxiliary textual supervision. They do not explicitly exploit the structural property of chest X-rays, where diagnostic information is spatially sparse yet globally organized. A self-supervised objective that captures holistic anatomical relationships without reconstruction overhead or augmentation-induced distortion therefore remains desirable.

To bridge this gap, we introduce S-PCL (Semantic-Partitioned Contrastive Learning), a simple yet effective self-supervised framework tailored for chest X-ray representation learning. Instead of reconstructing masked regions or relying on hand-crafted augmentations, S-PCL constructs two complementary views by randomly partitioning image patches into non-overlapping subsets within a single image. By maximizing agreement between these partitioned views, the encoder is encouraged to infer missing contextual information and capture coherent global thoracic structure. Such a design promotes the modeling of clinically meaningful anatomical relationships, for example, the spatial dependency between lung fields and ribs, while avoiding pixel-level redundancy and unnecessary semantic distortion. Our main contributions are summarized as follows:

1) We introduce S-PCL, a streamlined pre-training framework that integrates the efficiency of partition-based modeling with the discriminative power of contrastive learning, avoiding reconstruction overhead and augmentation-induced distortion.

2) We show that contrasting non-overlapping partitions enables efficient learning of high-level diagnostic representations without auxiliary components such as momentum encoders or complex decoders.

3) Extensive experiments on large-scale CXR datasets demonstrate state-of-the-art downstream performance and favorable scaling efficiency.

2 Methodology

2.1 Method Overview

Avoiding aggressive hand-crafted augmentations, S-PCL executes its self-supervised task in three steps (see Figure 1). 1) tokenizing and randomly masking the input radiograph; 2) splitting the visible tokens into disjoint subsets to create parallel contrastive views; and 3) passing these views through a shared Vision Transformer to optimize a T-distributed spherical contrastive loss.

To formalize this pipeline, we first detail the initial tokenization stage. Given an input CXR image $\mathbf{x} \in \mathbb{R}^{H \times W \times 1}$, we follow the standard Vision Transformer (ViT) protocol by reshaping it into a sequence of 2D patches $\mathbf{x}_p \in \mathbb{R}^{N \times P^2}$, where (H, W) denotes the original image resolution, P represents the patch size, and $N = HW/P^2$ indicates the total number of patches. These patches are subsequently mapped via a linear projection into D-dimensional embeddings and combined with fixed sinusoidal positional embeddings $\mathbf{p} \in \mathbb{R}^{N \times D}$ to preserve the thoracic anatomical layout. Consequently, this yields a token sequence $\mathbf{E} = \text{Linear}(\mathbf{x}_p) + \mathbf{p} \in \mathbb{R}^{N \times D}$ encapsulating the fine-grained semantics of the image before the masking operation. This unmasked sequence $\mathbf{E}$ establishes the foundational representation from which we derive our computationally efficient contrastive views, as detailed in the subsequent masking strategy.

2.2 Semantic-Partitioned Masking Strategy

Medical images inherently exhibit significant conceptual redundancy. While various patches within a single radiograph display distinct visual characteristics, they are all fundamentally interconnected with the overall clinical meaning of the image. Instead of reconstructing masked pixels as in standard Masked Image Modeling (MIM), our strategy utilizes random sampling without replacement following a uniform distribution to initially mask the image.

Given a global masking ratio r (e.g., 30%), the remaining $n = \lfloor (1-r)N \rfloor$ visible patches are retained to capture the comprehensive anatomical structure. To construct the contrastive views, these visible patches are randomly partitioned into two non-overlapping groups $\mathcal{V}_1, \mathcal{V}_2 \in \mathbb{R}^{\frac{n}{2} \times D}$. This random, non-overlapping division ensures that the central positions of the visible patches remain statistically consistent across both groups while actively avoiding potential spatial biases.

Crucially, this strategy creates a deliberate dual-ratio effect. While the global masking ratio remains low to capture overall relationships, the disjoint partitioning means each contrastive branch effectively experiences a much higher masking ratio (e.g., 65%). During each forward pass, the model observes only a severely restricted portion of the visible tokens. This challenging scenario forces the model to focus on localized pathological features rather than relying on simple patterns or redundant information, thereby creating diverse views with substantial fine-grained semantic differences at the concept level.

2.3 Efficient Contrastive Learning

Following the generation of the disjoint subsets $\mathcal{V}_1$ and $\mathcal{V}_2$, we prepend a learnable `[CLS]` token to each sequence. Both subsets are then fed independently into a shared Vision Transformer encoder, denoted as $f_\theta(\cdot)$. Let $\mathbf{z}_1 = f_\theta(\mathcal{V}_1)$ and $\mathbf{z}_2 = f_\theta(\mathcal{V}_2)$ represent the high-level embeddings extracted from the respective `[CLS]` tokens, as these tokens aggregate the high-level semantic information of each partitioned view. By processing these non-overlapping views independently, the framework establishes a strict internal information bottleneck. The encoder's self-attention mechanism is heavily constrained, forcing it to aggregate long-range dependencies across the thoracic cavity and implicitly infer both the global anatomical layout and localized pathological anomalies from severely partial visual evidence.

To optimize the encoder, we apply a contrastive learning objective that maximizes the representational agreement between the paired semantic partitions. For a given mini-batch containing N CXR images, the masking and encoding process yields $2N$ representations. The embeddings $\mathbf{z}_1$ and $\mathbf{z}_2$ originating from the same radiograph constitute a positive pair, while the remaining $2(N-1)$ representations within the same batch serve as negative samples. In terms of similarity computation, we introduce the T-distributed spherical (T-SP) metric to significantly promote the intraclass compactness and interclass separability of features. Given the cosine distance $\cos(\mathbf{z}_1, \mathbf{z}_2)$ between the two normalized feature vectors, the T-SP similarity is defined as:

$$sim_{tsp}(\mathbf{z}_1, \mathbf{z}_2) = 0.5 \times \frac{1 + \cos(\mathbf{z}_1, \mathbf{z}_2)}{1 + (1 - \cos(\mathbf{z}_1, \mathbf{z}_2)) \times \kappa} \tag{1}$$

where $\kappa > 0$ denotes the concentration hyperpa rameter of the T-SP metric. We concurrently maximize the similarity of positive pairs while minimizing the similarity of negative examples to drive the network. The loss function for a

Table 1: **Comparison of our method with specialist approaches for disease classification.** Performance is measured using macro-averaged AUC. The labeling ratio X% indicates the proportion of the fully annotated training set used for supervised fine-tuning. Best results are highlighted in bold.

Method	GFLOPs	GPU Hrs	ChestX-ray14			CheXpert			RSNA Pneu.		
			1%	10%	100%	1%	10%	100%	1%	10%	100%
Training with clinical reports											
M3AE [9]	34.4	710	-	-	-	86.2	87.3	87.9	89.0	90.8	92.3
REFERS [14]	54.8	-	76.7	80.9	84.7	87.2	88.1	88.2	89.4	91.6	92.7
MRM [27]	13.1	800	79.4	84.0	85.9	88.5	88.5	88.7	91.3	92.7	93.3
Training without clinical reports											
SimCLR [6]	8.2	830	-	-	-	-	-	-	70.1	80.2	84.9
Medical MAE [8]	20.3	1200	-	-	82.3	-	-	89.2	-	-	-
CheXWorld [33]	67.4	-	-	-	83.5	-	-	**89.6**	-	-	75.0
S-PCL (Ours)	**6.1**	**540**	**78.2**	**82.1**	**84.1**	**86.7**	**88.4**	89.1	**86.6**	**89.2**	**91.2**

positive pair is formulated as:

$$\mathcal{L} = -\log \frac{\exp(sim_{tsp}(\mathbf{z}_1, \mathbf{z}_2) \times \tau)}{\sum_{j=1}^{2N} \mathbb{1}_{[j \neq 1]} \exp(sim_{tsp}(\mathbf{z}_1, \mathbf{z}_j) \times \tau)} \tag{2}$$

where τ is a trainable temperature parameter used to effectively scale the different samples, and $\mathbb{1}$ is an indicator function evaluating to 1 when the condition is met. This objective effectively enhances the intraclass conceptual compactness within a single radiograph and the interclass semantic separability across different patients in the mini-batch.

This semantic-partitioned contrastive design (S-PCL) is highly efficient. By defining the pre-training objective purely in latent space via representation alignment, it avoids the pixel-level reconstruction overhead. In contrast, standard MIM often overemphasizes high-frequency details and local features, which can diverge from the goal of learning high-level semantic concepts and reduce pre-training efficiency. Moreover, unlike many contrastive frameworks that require heavy pre-processing or auxiliary networks to create views, S-PCL uses the ViT `[CLS]` token directly, without momentum encoders, projection MLP heads, or decoders. This streamlined design reduces computation and memory, achieving the lowest GFLOPs among comparable SSL methods and scaling well to large clinical datasets.

3 Experiments

3.1 Datasets and Implementation Details

Datasets. We use **MIMIC-CXR-JPG[28]** for self-supervised pre-training. Following a 7:2:1 train-validation-test split across all downstream tasks, we evaluate our model on the following benchmarks: 1) **ChestX-ray14[29]**, containing 112,120 radiographs with 14 pathology labels for multi-label classification. 2) **CheXpert [30]**, comprising 224,316 images with 14 observations for multi-label classification. 3) **RSNA Pneumonia [31]**, containing approximately 30,000 images annotated for pulmonary opacity. 4) **SIIM-ACR Pneumothorax[32]**, consisting of over 12,000 radiographs with pixel-level masks for semantic segmentation.

Pre-training and Fine-tuning Settings. We employed a ViT-Base backbone using 16×16 patches, which encodes input images of size 512×512 into a sequence of patch tokens. During each forward pass, a random subset of patch tokens is masked at a ratio of 0.6, and the remaining visible tokens are split into two non-overlapping views that are independently encoded by the shared ViT encoder. A contrastive loss is then computed between the `[CLS]` token representations of the two branches. We used a mini-batch size of 600 per GPU with gradient accumulation over 2 iterations. Furthermore, we follow the fine-tuning settings of Medical MAE[8]. To ensure consistency, all training and inference times are measured using a single NVIDIA RTX A6000 GPU.

3.2 Comparison with State-of-the-art Methods

Figure 2 shows that among the compared methods, S-PCL achieves the lowest pre-training cost (540 GPU hours) while maintaining competitive fine-tuning performance (89.1% mAUC). In contrast, Medical MAE requires the most

Table 2: **Performance comparison on the CheXpert benchmark**. We report the Area Under the Curve (AUC) for five clinical observations and their mean (mAUC). Best results are highlighted in bold.

Method	Backbone	Atelectasis	Cardiomegaly	Consolidation	Edema	Effusion	mAUC (%)
Label-Assemble [34]	DN121	82.1	85.9	**94.4**	89.2	93.6	89.0
Medical MAE [8]	ViT-B/16	**82.7**	83.5	92.5	93.8	94.1	**89.3**
S-PCL (Ours)	ViT-B/16	80.3	**95.4**	80.4	**94.1**	**95.6**	89.1

Table 3: **Performance comparison on the ChestX-ray14 benchmark.** We report the AUC scores across all 14 categories. The best results are in bold and the second-best results are underlined.

Model	Mean	Atelectasis	Cardiomegaly	Effusion	Infiltration	Mass	Nodule	Pneumonia	Pneumothorax	Consolidation	Edema	Emphysema	Fibrosis	Pleural Thicken	Hernia
ConVIRT[17]	56.0	45.1	44.3	63.2	65.1	61.6	57.2	63.6	54.1	63.7	70.2	41.9	47.4	56.0	51.2
GLoRIA[18]	81.8	82.6	83.3	86.0	66.4	81.8	73.5	71.0	84.5	81.3	89.8	93.1	78.9	76.1	**97.5**
MRM [27]	**85.9**	**84.2**	**93.0**	89.6	71.8	**88.2**	**78.5**	77.3	90.2	**82.2**	**91.0**	**94.3**	**86.7**	**81.4**	94.4
S-PCL (Ours)	84.1	82.3	87.7	**91.4**	**75.7**	80.8	75.0	**77.3**	**92.5**	79.0	89.4	93.5	82.6	80.1	90.3

pre-training resources (1200 GPU hours) for a marginal performance gain (89.2% mAUC), and MRM offers a balanced trade-off with 800 GPU hours and 88.7% mAUC. This suggests that S-PCL is more efficient in pre-training without significant sacrifice in downstream accuracy. Furthermore, employing ViT-S/16 as the backbone, our S-PCL reaches 82.8% mAUC on the CheXpert dataset, requiring only 140 GPU hours for pre-training.

Table 1 shows that S-PCL achieves competitive performance across all three chest X-ray datasets under different fine-tuning ratios. On ChestX-ray14, S-PCL attains 78.2%, 82.1%, and 84.1% AUC with 1%, 10%, and 100% of the training data, respectively. On CheXpert, it reaches 86.7%, 88.4%, and 89.1% AUC, while on RSNA Pneumonia, it obtains 86.6%, 89.2%, and 91.2% AUC.

Table 2 provides a detailed per-disease comparison on the CheXpert benchmark. S-PCL with a ViT-B/16 backbone achieves 89.1% mean AUC, which is competitive with the best-performing methods. Notably, S-PCL obtains the highest

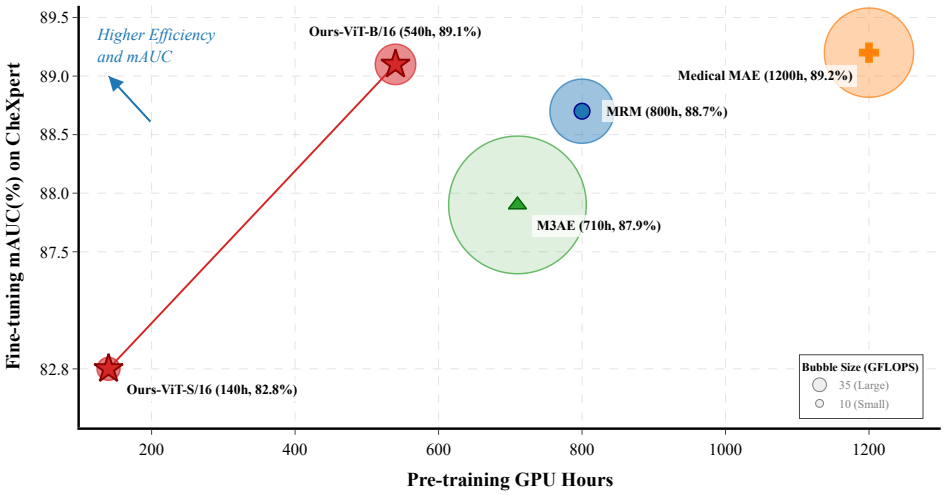

Figure 2: Efficiency and scaling comparison of MRM[27], Medical MAE[8], M3AE [9], and our method on CheXpert fine-tuning, measured by mAUC (%).

Table 4: **Results of semantic segmentation.** Best results are highlighted in bold. Each model is fine-tuned with 1%, 10%, 100% training data.

Methods	SIIM-ACR Pneumothorax		
	1%	10%	100%
GLoRIA [18]	37.4	57.1	64.0
MGCA [21]	49.7	59.3	64.2
MedKLIP [20]	**50.2**	60.8	63.9
S-PCL (Ours)	38.8	**61.7**	**65.1**

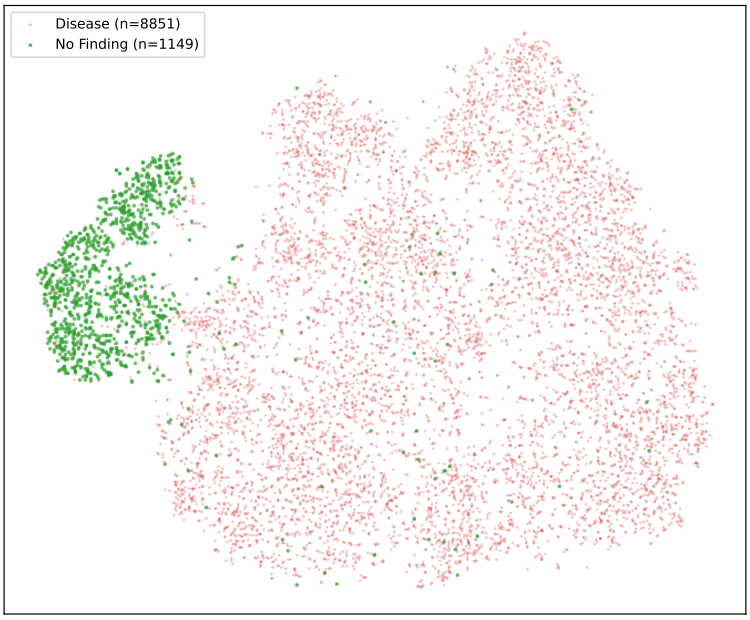

Figure 3: t-SNE visualization of the learned global representations on CheXpert benchmark.

AUC scores for Cardiomegaly (95.4%), Edema (94.1%), and Effusion (95.6%), outperforming all other approaches including Medical MAE variants. This demonstrates that S-PCL is particularly effective at learning representations for these specific thoracic conditions.

Table 3 expands our evaluation to the ChestX-ray14 dataset, detailing the model's diagnostic capabilities across 14 diverse thoracic pathologies. Our approach exhibits superior discriminative power in identifying specific localized conditions. Most notably, S-PCL excels in detecting complex anomalies such as Effusion (91.4%) and Pneumothorax (92.5%). These substantial gains indicate that forcing the encoder to infer global context from partitioned views effectively enhances its sensitivity to subtle, fine-grained pathological features compared to conventional contrastive frameworks.

Table 4 further demonstrates that S-PCL achieves competitive performance on semantic segmentation benchmark. The improvements are particularly evident in the 10% and 100% supervision settings, indicating strong dense prediction capability compared to prior vision–language pretraining methods.

3.3 Feature Interpretability

To interpret the learned representations, we visualize the high-dimensional features of 10,000 test images using t-SNE. We extract the global representations for 8,851 scans with diseases and 1,149 normal scans. Figure 3 reveals a clear separation between pathological and normal radiographs. This demonstrates that by enforcing agreement between incomplete semantic partitions, S-PCL implicitly discovers highly discriminative and interpretable clinical concepts without relying on any explicit annotations.

4 Conclusion

We introduce S-PCL, a pre-training paradigm for CXRs that eliminates pixel-level reconstruction and risky augmentations by contrasting semantic-partitioned views. By exploiting inherent medical imaging redundancy, S-PCL efficiently learns robust representations from partial observations. This significantly reduces computational overhead while outperforming state-of-the-art baselines, paving the way for scalable learning in high-resolution medical foundation models.

References

[1] Liang Chen, Paul Bentley, Kensaku Mori, Kazunari Misawa, Michitaka Fujiwara, and Daniel Rueckert. Self-supervised learning for medical image analysis using image context restoration. *Medical image analysis*, 58:101539, 2019.

[2] Xiaoyu Yang, Lijian Xu, Xingyu Zeng, Xiaosong Wang, Hongsheng Li, and Shaoting Zhang. Scalar: Spatial-concept alignment for robust vision in harsh open world. *Pattern Recognition*, 2026.

[3] Hong-Yu Zhou, Shuang Yu, Cheng Bian, Yifan Hu, Kai Ma, and Yefeng Zheng. Comparing to learn: Surpassing imagenet pretraining on radiographs by comparing image representations. In *International Conference on Medical Image Computing and Computer-Assisted Intervention*, pages 398–407. Springer, 2020.

[4] Xiaoyu Yang, Lijian Xu, Simon Yu, Qing Xia, Hongsheng Li, and Shaoting Zhang. Geometry-based end-to-end segmentation of coronary artery in computed tomography angiography. In *International Workshop on Trustworthy Machine Learning for Healthcare*, pages 190–196. Springer, 2023.

[5] Che Liu, Sibo Cheng, Chen Chen, Mengyun Qiao, Weitong Zhang, Anand Shah, Wenjia Bai, and Rossella Arcucci. M-flag: Medical vision-language pre-training with frozen language models and latent space geometry optimization. In *International conference on medical image computing and computer-assisted intervention*, pages 637–647. Springer, 2023.

[6] Ting Chen, Simon Kornblith, Mohammad Norouzi, and Geoffrey Hinton. A simple framework for contrastive learning of visual representations. In *International conference on machine learning*, pages 1597–1607. PmLR, 2020.

[7] Xiaoyu Yang, Lijian Xu, Hongsheng Li, and Shaoting Zhang. One leaf reveals the season: Occlusion-based contrastive learning with semantic-aware views for efficient visual representation. In *Forty-second International Conference on Machine Learning*, 2025.

[8] Junfei Xiao, Yutong Bai, Alan Yuille, and Zongwei Zhou. Delving into masked autoencoders for multi-label thorax disease classification. In *Proceedings of the IEEE/CVF Winter Conference on Applications of Computer Vision*, pages 3588–3600, 2023.

[9] Zhihong Chen, Yuhao Du, Jinpeng Hu, Yang Liu, Guanbin Li, Xiang Wan, and Tsung-Hui Chang. Multi-modal masked autoencoders for medical vision-and-language pre-training. In *International Conference on Medical Image Computing and Computer-Assisted Intervention*, pages 679–689. Springer, 2022.

[10] Lijian Xu, Ziyu Ni, Hao Sun, Hongsheng Li, and Shaoting Zhang. A foundation model for generalizable disease diagnosis in chest x-ray images. *arXiv preprint arXiv:2410.08861*, 2024.

[11] Lijian Xu, Hao Sun, Ziyu Ni, Hongsheng Li, and Shaoting Zhang. Medvilam: A multimodal large language model with advanced generalizability and explainability for medical data understanding and generation. *arXiv preprint arXiv:2409.19684*, 2024.

[12] Linshan Wu, Jiaxin Zhuang, and Hao Chen. Large-scale 3d medical image pre-training with geometric context priors. *IEEE Transactions on Pattern Analysis and Machine Intelligence*, 2025.

[13] Xiaoyu Yang, Lijian Xu, Simon Yu, Qing Xia, Hongsheng Li, and Shaoting Zhang. Segmentation and vascular vectorization for coronary artery by geometry-based cascaded neural network. *IEEE Transactions on Medical Imaging*, 2024.

[14] Hong-Yu Zhou, Xiaoyu Chen, Yinghao Zhang, Ruibang Luo, Liansheng Wang, and Yizhou Yu. Generalized radiograph representation learning via cross-supervision between images and free-text radiology reports. *Nature Machine Intelligence*, 4(1):32–40, January 2022.

[15] Weijian Huang, Cheng Li, Hong-Yu Zhou, Hao Yang, Jiarun Liu, Yong Liang, Hairong Zheng, Shaoting Zhang, and Shanshan Wang. Enhancing representation in radiography-reports foundation model: a granular alignment algorithm using masked contrastive learning. *Nature Communications*, 15(1):7620, 2024.

[16] Lijian Xu, Ziyu Ni, Xinglong Liu, Xiaosong Wang, Hongsheng Li, and Shaoting Zhang. Learning a multi-task transformer via unified and customized instruction tuning for chest radiograph interpretation. *arXiv preprint arXiv:2311.01092*, 2023.

[17] Yuhao Zhang, Hang Jiang, Yasuhide Miura, Christopher D Manning, and Curtis P Langlotz. Contrastive learning of medical visual representations from paired images and text. In *Machine Learning for Healthcare Conference*, pages 2–25. PMLR, 2022.

[18] Shih-Cheng Huang, Liyue Shen, Matthew P Lungren, and Serena Yeung. Gloria: A multimodal global-local representation learning framework for label-efficient medical image recognition. In *Proceedings of the IEEE/CVF International Conference on Computer Vision*, pages 3942–3951, 2021.

[19] Benedikt Boecking, Naoto Usuyama, Shruthi Bannur, Daniel C Castro, Anton Schwaighofer, Stephanie Hyland, Maria Wetscherek, Tristan Naumann, Aditya Nori, Javier Alvarez-Valle, et al. Making the most of text semantics to improve biomedical vision–language processing. In *European conference on computer vision*, pages 1–21. Springer, 2022.

[20] Chaoyi Wu, Xiaoman Zhang, Ya Zhang, Yanfeng Wang, and Weidi Xie. Medklip: Medical knowledge enhanced language-image pre-training for x-ray diagnosis. In *ICCV*, pages 21372–21383, 2023.

[21] Fuying Wang, Yuyin Zhou, Shujun Wang, Varut Vardhanabhuti, and Lequan Yu. Multi-granularity cross-modal alignment for generalized medical visual representation learning. *Advances in neural information processing systems*, 35:33536–33549, 2022.

[22] Shawn Young, Xingyu Zeng, and Lijian Xu. Fewer tokens, greater scaling: Self-adaptive visual bases for efficient and expansive representation learning. *arXiv preprint arXiv:2511.19515*, 2026.

[23] Landi He, Xiaoyu Yang, and Lijian Xu. The model knows which tokens matter:automatic token selection via noise gating. *arXiv preprint*, 2026.

[24] Zhuo Chen, Shawn Young, and Lijian Xu. Tc-ssa: Token compression via semantic slot aggregation for gigapixel pathology reasoning. *arXiv preprint arXiv:2603.01143*, 2026.

[25] Yonghan Gao, Zehong Chen, Lijian Xu, Jingzhi Chen, Jingwei Guan, and Xingyu Zeng. Zerosense: How vision matters in long context compression. *arXiv preprint arXiv:2603.7337970*, 2026.

[26] Peihang Wu and Lijian Xu. Towards efficient multimodal large language models of gigapixel pathology: A survey on token compression. *arXiv preprint*, 2026.

[27] Hong-Yu Zhou, Chenyu Lian, Liansheng Wang, and Yizhou Yu. Advancing radiograph representation learning with masked record modeling. In *The Eleventh International Conference on Learning Representations*, 2023.

[28] AEWP Johnson, Tom Pollard, Roger Mark, Seth Berkowitz, and Steven Horng. Mimic-cxr database. *PhysioNet10*, 13026:C2JT1Q, 2019.

[29] Xiaosong Wang, Yifan Peng, Le Lu, Zhiyong Lu, Mohammadhadi Bagheri, and Ronald M Summers. Chestx-ray8: Hospital-scale chest x-ray database and benchmarks on weakly-supervised classification and localization of common thorax diseases. In *Proceedings of the IEEE conference on computer vision and pattern recognition*, pages 2097–2106, 2017.

[30] Jeremy Irvin, Pranav Rajpurkar, Michael Ko, Yifan Yu, Silviana Ciurea-Ilcus, Chris Chute, Henrik Marklund, Behzad Haghgoo, Robyn Ball, Katie Shpanskaya, et al. Chexpert: A large chest radiograph dataset with uncertainty labels and expert comparison. In *Proceedings of the AAAI conference on artificial intelligence*, volume 33, pages 590–597, 2019.

[31] George Shih, Carol C Wu, Safwan S Halabi, Marc D Kohli, Luciano M Prevedello, Tessa S Cook, Arjun Sharma, Judith K Amorosa, Veronica Arteaga, Maya Galperin-Aizenberg, et al. Augmenting the national institutes of health chest radiograph dataset with expert annotations of possible pneumonia. *Radiology: Artificial Intelligence*, 1(1):e180041, 2019.

[32] Society for imaging informatics in medicine: Siim-acr pneumothorax segmentation. `https://www.kaggle.com/c/siim-acr-pneumothorax-segmentation`. 2019.

[33] Yang Yue, Yulin Wang, Chenxin Tao, Pan Liu, Shiji Song, and Gao Huang. Chexworld: Exploring image world modeling for radiograph representation learning. In *Proceedings of the Computer Vision and Pattern Recognition Conference*, pages 20778–20788, 2025.

[34] Mintong Kang, Bowen Li, Zengle Zhu, Yongyi Lu, Elliot K Fishman, Alan Yuille, and Zongwei Zhou. Label-assemble: Leveraging multiple datasets with partial labels. In *2023 IEEE 20th International Symposium on Biomedical Imaging (ISBI)*, pages 1–5. IEEE, 2023.